coatings

MDPI

Article

The Properties of Binary and Ternary Ti Based Coatings Produced by Thermionic Vacuum Arc (TVA) Technology

Aurelia Mandes [1], Rodica Vladoiu [1,*], Gabriel Prodan [1], Virginia Dinca [1], Corneliu Porosnicu [2] and Paul Dinca [2]

[1] Faculty of Applied Sciences and Engineering, Ovidius University, 124 Mamaia Av., 900527 Constanţa, Romania; amandes@univ-ovidius.ro (A.M.); gprodan@univ-ovidius.ro (G.P.); vdinca@univ-ovidius.ro (V.D.)

[2] National Institute for Laser, Plasma and Radiation Physics,409 Atomistilor Av., P.O. Box MG-36, 077125 Magurele, Bucharest, Romania; corneliu.porosnicu@inflpr.ro (C.P.); paul.dinca@inflpr.ro (P.D.)

* Correspondence: rvladoiu@univ-ovidius.ro; Tel./Fax: +40-241-618-372

Received: 7 February 2018; Accepted: 16 March 2018; Published: 20 March 2018

Abstract: A series of the multicomponent thin films (binary: Ti-C; Ti-Ag and ternary: Ti-C-Ag; Ti-C-Al) were fabricated by Thermionic Vacuum Arc (TVA) technology in order to study the wear resistance and the anticorrosion properties. The effects of Ti amount on the microstructure, tribological and morphological properties were subsequently investigated. TVA is an original deposition method using a combination of anodic arc and electron gun systems for the growth of films. The samples were characterized using scanning electron microscope (SEM) and a transmission electron microscope (TEM) accompanied by selected area electron diffraction (SAED). Tribological properties were studied by a ball-on-disc tribometer in the dry regime and the wettability was assessed by measuring the contact angle with the See System apparatus. Wear Rate results indicate an improved sliding wear behavior for Ti-C-Ag: 1.31×10^{-7} mm^3/N m (F = 2 N) compared to Ti-C-Al coating wear rate: 4.24×10^{-7} mm^3/N m. On the other hand, by increasing the normal load to 3 N an increase to the wear rate was observed for Ti-C-Ag: 2.58×10^{-5} mm^3 compared to 2.33×10^{-6} mm^3 for Ti-C-Al coating.

Keywords: Ti based coatings; Thermionic Vacuum Arc (TVA); tribological properties; TEM characterization

1. Introduction

Surface engineering is quickly developing such that the surface modification of widespread used materials allows us to transform a material with poor properties into a functional product. The uses for titanium in industry are growing faster than ever before, as a material that is both strong and lightweight. Titanium also has many outstanding properties such as being excellent in corrosion resistance (even in seawater), high in strength (~1800 MPa), high in electric resistance, and excellent in biocompatibility [1–3]. These properties allow it to be used in numerous applications in the aerospace industry, building industry, sports material industry and as implants in a number of surgical procedures [4–6].

Unfortunately, titanium is prone to wear because of its limited tribological properties, antifriction characteristics and the low hardness of the material restricts its use in engineering applications. In order to increase the material stiffness, it is often used in metal matrix composites. When titanium is "mixed" with other metals, advanced materials with amazing properties could be revealed and, from the economic point of view, the price of final products would be decreased, which might be of particular advantage for industrial applications.

Starting from this idea, we focused on the binary (Ti-C and Ti-Ag) and ternary (Ti-C-Ag and Ti-C-Al) thin films with different Ti contents. For instance, Ti-C thin films exhibit remarkable properties like high hardness values, high melting points, high thermal and electrical conductivity coefficients and low friction [7–10]. Because of their unique properties, they are increasingly used as corrosion-resistant and wear films on cutting tools and diffusion barrier in semiconductor technology. Besides, their high melting point also makes them suitable coatings to be used as first wall material in fusion reactors [11–13]. On the other hand, silver and silver-based compounds are known not only as efficient antibacterial agents having a large spectrum of activity [14–16] but furthermore, in wear situations, the inclusion of silver into Ti compounds can improve their properties by acting as a solid lubricant [17–19]. The superiority of aluminum matrix composite materials over conventional ones inspired us to use them in ternary depositions. Their excellent friction and wear resistance, high elastic modulus, high strength and low heat expansion coefficients are the remarkable properties of the Ti-C-Al thin films [20–24]. In addition, in order to reduce the contact resistance further and afford for applications at low currents and loads, Ag was added to the ternary (Ti-C-Ag) coating [25,26].

The general aim of this work is to study at the nanoscale effects of Ti content on the mechanical behavior of composite films that could admit their optimization for advanced engineering applications, especially for gear wheals and camshafts coating as mechanical components of irrigation pumps. The main challenge is to find the best combination for increasing the wear resistance and the anticorrosion properties. The binary and ternary thin films were deposited by TVA technology, an original method for deposition of high purity thin films suitable for nanostructured film synthesis of any solid materials.

2. Materials and Methods

The TVA method uses an electron beam emitted by an externally heated cathode accelerated by a high anodic voltage [27–29]. A Wehnelt cylinder is used to focus the electrons on the anode surface. The electron beam can evaporate the anode materials as neutral pure particles and facilitate their deposition on the substrate when the electron energy and current intensity are not too high. By increasing the anode potential up to a certain value, the evaporation rate rises enough to allow a bright discharge to be ignited in the evaporated pure material. Because the discharge sustaining gas is just the evaporating atoms in a vacuum without any other inert buffer gas, the thin film deposition is carried out in high purity conditions. More details are presented elsewhere [30–32]. In this way, it is possible to meaningfully refine the quality of the surfaces coated with different materials.

One of the important advantages of this method is the fact that TVA allows the simultaneous deposition of different materials in the same time as can be seen in Figure 1 [33]. The electron beams provided from two or three guns depending on the purpose of mixture—which can operate independently—might evaporate in materials contained in the crucible, used as anodes. In the case of carbon, instead of a crucible filled with grains of the material, a carbon rod of 10 mm is used. The anodes are symmetrically arranged with respect to the vessel axis.

Binary and ternary composite films (Ti-99.99%, Ag-99.9%, Al-99.99% purity—metal basis) obtained on three types of substrates were used in this work: glass, silicon wafer and OLC 45. In the presented paper, the interest is focused on the special substrate OLC 45 (high-quality carbon steel with 0.45% C) requested by a specific industrial application interest. Before fixing the sample on the holder, these substrates are cleaned in order to remove surface contaminations. Ultrasonic bath with a highly effective cleaner (acetone) is usually the cleaning method.

The main operating parameters during the deposition process are listed in Table 1 including the rate of deposition, final thickness for each evaporated material and the average pressure during the coating process, where: I_f—the current intensity of the heating filament; U_a—the applied high voltage over the electrodes; I_a—the arc current intensity.

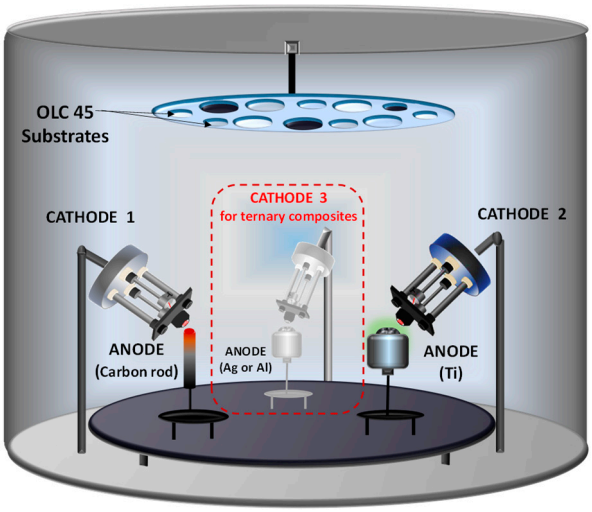

Figure 1. The schematic view of the experimental set-up.

Table 1. The parameters for ternary and binary thin film synthesis.

Parameters	Ternary						Binary	
	Ti-C-Ag			Ti-C-Al			Ti-C	Ti-Ag
	C	Ti	Ag	C	Ti	Al		
I_f (A)	76	38	36	76	38	38	57	54
U_a (kV)	2.0	0.8	1.1	2.0	0.8	1.3	1.35	0.8
I_a (A)	1.00	1.12	0.30	1.0	1.12	0.5	0.3	0.7
Rate of deposition (Å/s)	0.76			0.86			0.06	0.05
Thickness (nm)	400			1800			125	100
Pressure during deposition (Pa)	2.6×10^{-3}			9.9×10^{-4}			7.0×10^{-4}	6.0×10^{-4}

The deposition rate and thickness for each material were monitored in situ during the entire process with the use of micro-quartz balances. The thickness of the composite layer was obtained by summing the corresponding thickness for each material. During the coating process the substrates were radiatively heated by the hot anode materials (203 °C for Ti-C-Ag and 225 °C for Ti-C-Al).

Electron Microscope (Philips CM120ST100kV (Philips, Eindhoven, The Netherlands) and SuperTWIN Objective Lens (Philips, Eindhoven, The Netherlands) was used for Transmission Electron Microscopy (TEM) and Selected Area Electron Diffraction (SAED) techniques to acquire images for morphological and structural investigation. Structural analysis was performed with the Scanning electron microscope EVO 50 XVP (Carl Zeiss NTS, Jena, Germany) with EDX attachment (Bruker, Jena, Germany). In addition, the tribological properties were studied by ball-on-disc tribometer made by CSM Switzerland in the dry regime.

3. Results

Tribological measurements were performed using a ball-on-disc tribometer, with a normal force of 1 N, 2 N and 3 N, respectively. The stainless-steel ball has a diameter of 6 mm, a dry sliding distance of 50 m, and a linear speed of 2 cm/s. Figure 2 shows a comparative view of the friction coefficient for Ti-C-Al and Ti-C-Ag films deposited on the substrate (OLC 45) at different loading forces. The OLC 45 substrates were provided by the industrial partner as used its own polishing process. Sample code 01 represents the OLC 45 substrate placed above the Ag respectively Al plasma source depending on the deposition type (Ti-C-Al, Ti-C-Ag); on the other hand, Sample code 09 represents the sample placed above the Ti plasma source. By positioning our samples in this manner, we inevitably obtain a

concentration gradient of each material in the layers. Since the distance between plasma sources and substrate holder is 40 cm, by comparison to holder diameter of 10 cm the amount of each material should not vary greatly in comparison to insitu measurements. However, we can see in Figure 2 that the sample 01 placed near the Ti plasma source has a higher friction coefficient in comparison to Sample Code 09, which means that the samples have different elemental ratios which in turn affect the sliding wear behavior.

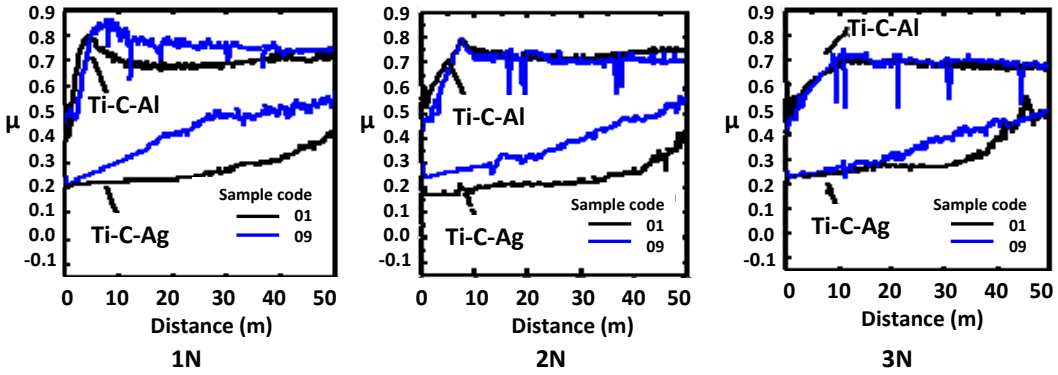

Figure 2. Friction coefficient for Ti-C-Al and Ti-C-Ag thin films deposited on OLC 45 (high-quality carbon steel with 0.45% C) substrate.

Ti-C-soft metal (Al/Ag) matrix was chosen to improve the sliding wear behavior. The use of soft metal had the purpose of retarding the wear of the steel substrate in order to prevent deformation and crack nucleation and to provide low shear conditions for good tribological properties. Since the sliding speed used for the measurements was 2 cm/s, we can surely assume that coatings wear did not occur due to an oxidative mechanism. A steep rising of the friction coefficient was observed for Ti-C-Al for all three normal loads used. This was most likely caused by the delamination through micro-cutting of the coating due to both the intense ploughing action of the stainless-steel ball together and the mating surface asperities. The delamination caused the formation of wear debris to further increase the ploughing and plastic deformation leading to an increased friction coefficient up to a point when the ball reached the substrate asperities leading to a fatigue delamination mechanism evidenced in the graphs by relatively constant friction coefficient. The value of the friction coefficient is typical for steel sliding against steel (0.7–0.8). At 3 N load, the film friction coefficient value becomes almost equal to the value of the substrate. On the other hand, a significant reduction of the friction coefficient value for Ti-C-Ag samples down to 0.2 has been obtained. So, in terms of friction reduction, Ti-C-Ag coatings provide an improvement in comparison to Ti-C-Al coatings.

SEM measurements were carried out for investigation of the morphology of the area and wear resistance in the cases of Ti-C-Ag/Ti-C-Al. As can be revealed from Figure 3, the traces of wear were much finer in the case of films containing Ag than those containing Al.

On the basis of depth profile measurements performed on the wearing traces, the wear rate was estimated for 1, 2 and 3N loading forces, respectively. In Figure 4, the depth profile of the wearing traces after the ball-on-disc tests on 3N loading force for Ti-C-Ag and Ti-C-Al film deposited on OLC 45 substrate can be seen.

For 1 N force, the wear rate could not be calculated due to the high roughness of the substrate. The wear rate for Ti-C-Ag thin film was 1.31×10^{-7} mm^3/N m for a force of 2 N while for 3 N is 2.58×10^{-5} mm^3/N m. In the case of Ti-C-Al coating, the wear rate was 4.24×10^{-7} mm^3/N m for a force of 2 N while for 3 N is higher: 2.33×10^{-6} mm^3/N m. These values as presented in Table 2 indicate a good behavior of the deposited layers under working conditions.

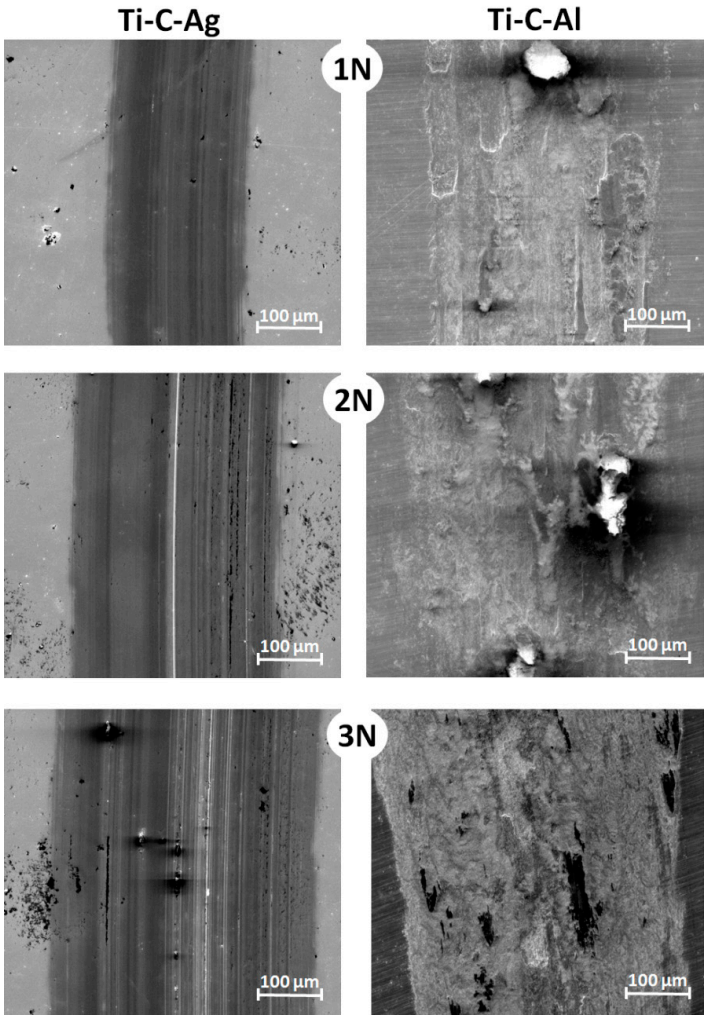

Figure 3. SEM images revealed from the wearing traces of Ti-C-Ag and Ti-C-Al thin films deposited on OLC 45 substrate.

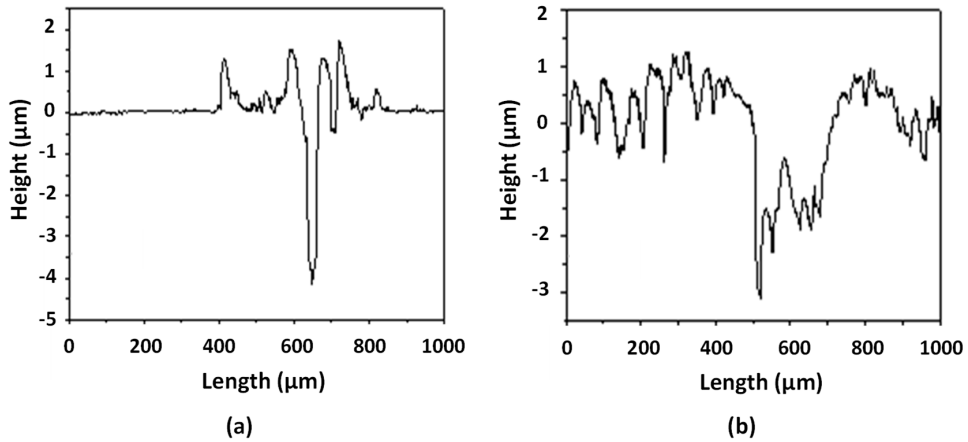

Figure 4. Depth profile of the wearing traces for Ti-C-Ag/OLC 45 (**a**) and Ti-C-Al/OLC 45 (**b**) after 3 N loading force.

Table 2. Area and wear rates of thin films.

Sample	Wear Area (μm²)	Wear Rate (mm³/N m)	Wear Area (μm²)	Wear Rate (mm³/N m)
	Loading Forces 2 N		Loading Forces 3 N	
Ti-C-Ag/OLC 45	6.05	1.31×10^{-7}	645.46	2.58×10^{-5}
Ti-C-Al/OLC 45	18.17	4.24×10^{-7}	58.37	2.33×10^{-6}

Calculation of the wear rate (K) is done using the following equation:

$$K = \frac{A \times L_{\text{ball}}}{F \times L_{\text{sliding}}} \left(\frac{\text{mm}^3}{\text{N m}} \right) \quad (1)$$

where: F—loading force(N); L_{sliding}—Length (m); A—area (mm²); L_{ball}—wear circumference (mm).

TEM characterizations revealed the morphological and structural features of the films. The 180k× working magnification has been performed to obtain useful information about particle/grain dimensions in ternary cases. For binary cases, 105k× magnification was setup. Mean diameter was evaluated from experimental data assuming a lognormal distribution of measured sizes, based on Equation (2):

$$y = y_0 + A \exp\left(\frac{\ln^2 \frac{x}{x_c}}{2w^2} \right) \quad (2)$$

where: A is an arbitrary constant; x_c is the maximum of the distribution.

TEM images presented in Figure 5 show the features of sample Ti-C-Ag/Si (Figure 5a) and Ti-C-Al/Si (Figure 5b) at 100 nm scale, together with FERET diameters histogram with log-normal fit used to evaluate particles/grain mean size.

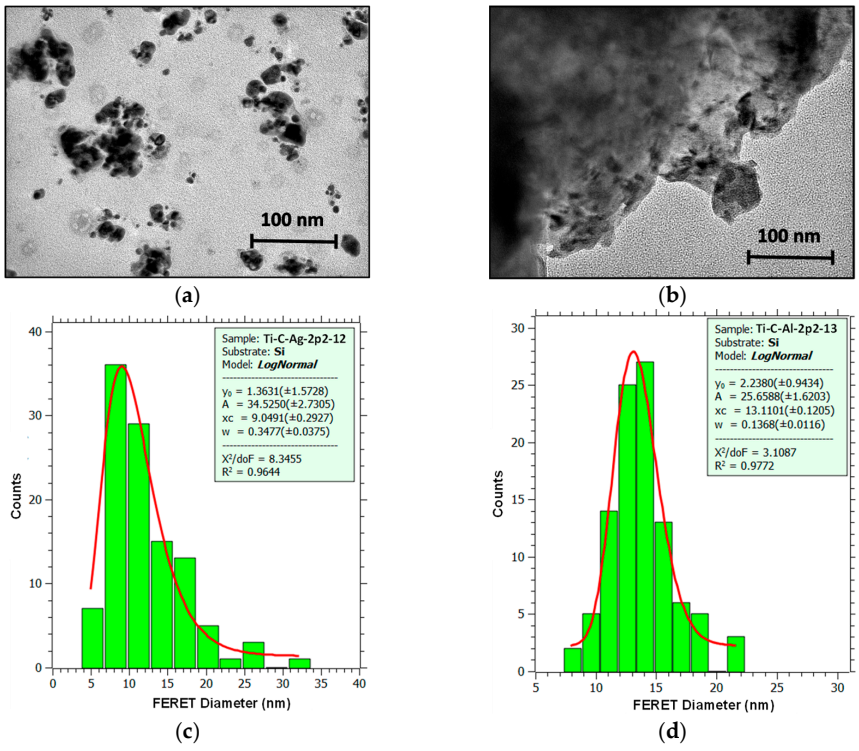

Figure 5. TEM images and grain size distribution and FERET diameters histogram of theTi-C-Ag/Si (**a**,**c**) and Ti-C-Al/Si (**b**,**d**).

SAED (Selected area electron diffraction) patterns (insets in Figure 6) show the polycrystalline feature of the samples. SAED profiles were extracted from these patterns using radial distribution function implemented in CRISP2 software and used to identify structural characteristics. The peaks from these profiles were fitted using a 9-degree polynomial function as background. In Figure 6a, the profile for Ti-C-Ag/Si shows that Ag cubic phase seems to be predominant. The second peak has a little shift from the correct position. The literature provides information about Ti-Ag alloys/compounds, with hexagonal [34] and tetragonal [35] structure. As we can see from reference peaks, between 0.8° and 1.2° there are possible superpositions of Ag [36], Ti [37], Ti-C [38], Ti-Ag phases. The hexagonal phase of Ti-Ag is difficult to identify because peaks are identical with peaks from hexagonal Ti. Furthermore, the first and second peaks from tetragonal Ti-Ag are missing, so we can eliminate this phase from the analysis. Carrying out Cohen analysis [39–42] for cubic Ag, we obtain a = 0.411 nm with a relative error about 0.605%. In the case of cubic Ti-C, lattice parameters are the same, but relative error is −5.3%. The hexagonal Ti has a = 0.2944 nm and c = 0.47437 nm, with relative error 0.84%, and 1.45%, respectively.

Scherrer formula applied to all identified peaks in the profile gives a crystallite size of about 4.08 nm. By comparing this with the value of 9.04 nm obtained from TEM images, we can conclude that the morphology of the Ti-C-Ag/Si sample is spherical monocrystalline particles, with the predominant phase being cubic Ag along with some crystalline cubic Ti-C and hexagonal Ti. Furthermore, the profile exhibits large background noise that can be associated with amorphous components from the sample and formvar support.

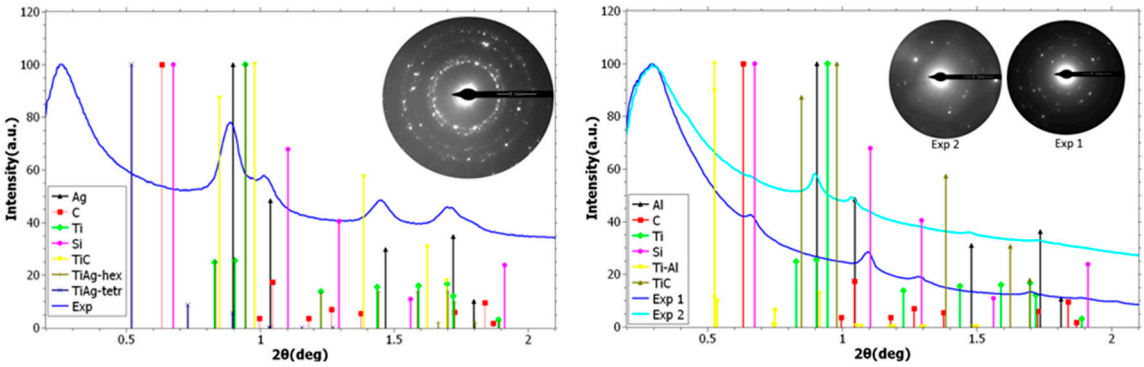

Figure 6. Radial distribution function and identified peaks in the profile of the Ti-C-Ag/Si (**a**) and Ti-C-Al/Si (**b**) films with SAED images (inset).

In the Ti-C-Al/Si case, the profiles were obtained in two different areas showing a different predominant phase, noted as Exp1 and Exp2 (inset Figure 6b). Exp1 area contains more Si (silicon phase with a = 0.5246 nm and −3.5% relative error) and Exp2 area contains a predominant cubic Al phase. As for the Ti-C-Al/Si sample, in the range between 0.8°–1.2°, we observe a peak superposition. Cohen analysis was performed assuming cubic Al; cubic Ti [43]; cubic Ti-C and hexagonal Ti show a large probability for Al phase and hexagonal Ti, but Ti-C are not excluded. The lattice parameter was a = 0.41664 nm, with relative error 2.8% for Al phase, and a = 0.5246 nm (−3.5% relative error) for cubic Si. For Ti-C, the lattice parameter was a = 0.4036 nm, with relative error −7.24%, which excludes the presence of this phase in the sample, and for the hexagonal Ti, a = 0.2916 nm and c = 0.4618 nm, with relative error −0.14% and −1.23%, respectively. The tetragonal structure of $Al_{2.5}Ti_{1.5}$ [44] was assumed and the result of Cohen analysis, performed even if the first peaks for this phase are missing, was a = 0.4102 nm and c = 0.3948 nm, with relative error 1.79% and −0.18%, respectively.

By applying the Scherrer formula to all identified peaks in the profile the crystallite size was found to be about 7.17 nm. Compared with the value of 13.04 nm obtained from TEM images, the similar spherical monocrystalline particles morphology for Ti-C-Al/Si sample as for Ti-C-Ag/Si case were

obtained. Structural analysis show that the predominant phase is cubic Al along with some crystalline tetragonal $Al_{2.5}Ti_{1.5}$ and hexagonal Ti. In addition, a large background noise exists in the profile that can be associated with amorphous components from the sample and formvar support.

Sample Ti-Ag/Si shows no crystalline components; the morphology of particles/grains presented in Figure 7a (experimentally identified peaks are marked on profile and values are characteristic to amorphous carbon). In contrast, the sample Ti-C/Si (Figure 7d) reveals a predominant cubic Ti-C phase, with lattice parameter determined by Cohen's method as a = 0.4098 nm with −5.59% relative error. Furthermore, both samples exhibit a lot of amorphous components.

The free surface energy (FSE) has been evaluated by means of Surface Energy Evaluation System (SEE System) using the contact angle method. By this measurement, we can evaluate the hydrophilicity or hydrophobicity of a thin film by determination of the tangent angle between the solid-vapor interface and liquid-solid interface. The testing liquids were water and ethylene glycol, and the free surface energy evaluation has been made on the basis of Wu equation of state model. The contact angle measurements have shown reproducible results for both binary and ternary thin films, as can be seen in Table 3.

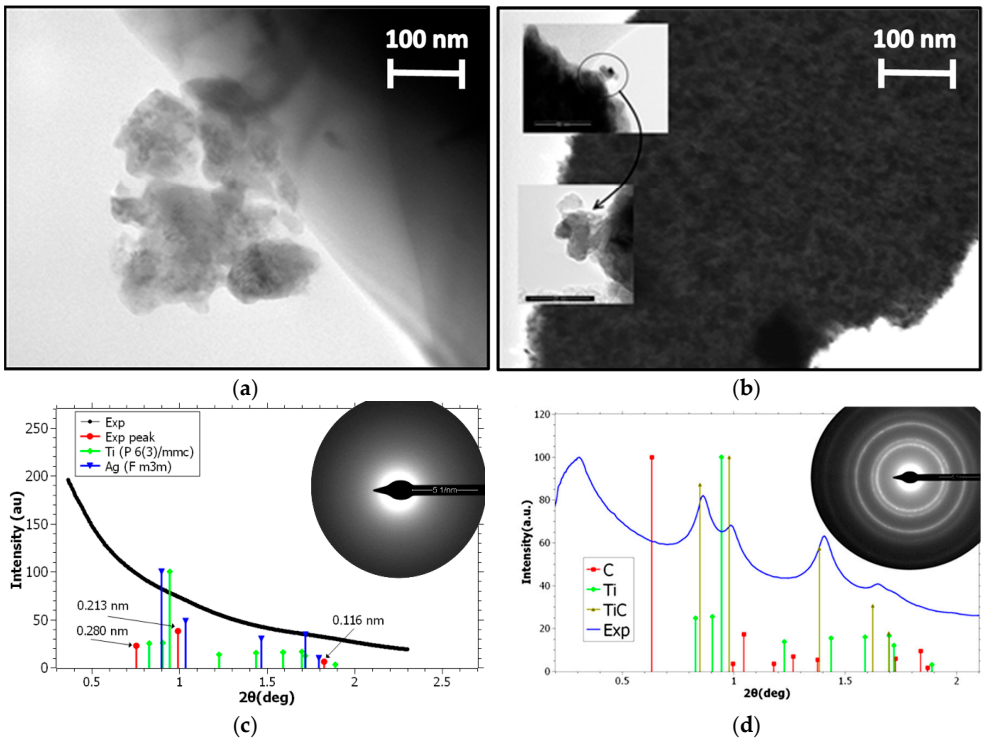

Figure 7. TEM images ((**a**) Ti-Ag/Si, (**b**) Ti-C/Si) and SAED profile ((**c**) Ti-Ag/Si, (**d**) Ti-C/Si) of the binary thin films.

Table 3. Contact angle and free surface energy measurements.

Samples	Contact Angle θ [°]		Free Surface Energy [mJ/m^2]
	Water	Ethylene Glycol	
Ti-C-Ag	137.18	86.16	13.66
Ti-C-Al	87.71	61.59	26.14
Ti-C	53.70	62.50	38.30
Ti-Ag	56.40	42.50	43.89

According to the Table 3, the obtained data for water contact angle of Ti-Ag and Ti-C films deposited on glass showed hydrophilic character. The measurements of contact angle using water as

liquid testing for ternary films revealed a drastic change of the wettability for Ti-C-Ag and Ti-C-Al deposited on glass. In addition, after one month of testing of the coated pieces in seawater and salted water (55% salt) by the industrial partner (24 h/day), the results indicated that both materials (Ag and C embedded in Ti) in contact with liquids would improve the anticorrosion behavior.

From the above results regarding the free surface energy, the influence of the third element in the thin film formation and how this element increased the contact angle value can be easily noticed, changing the character of the surface from hydrophilic to hydrophobic. The free surface energy of a solid has a decisive effect on its wettability. Its knowledge also enables the contact angle, the work of adhesion and the interfacial tension with liquids with known properties to be roughly predicted. This information is relevant for processes such as coating, solid lubricant, corrosion-resistant and wear films.

4. Conclusions

Complex characterization of the binary (Ti-C and Ti-Ag) and ternary (Ti-C-Ag/Si and Ti-C-Al/Si) thin films deposited by the TVA method has been performed. TEM and SEM images revealed high uniformity and smoothness in the mean range of 1.1 nm. The morphology of the Ti-C-Ag/Si sample is spherical monocrystalline particles, with the predominant phase being cubic Ag along with some crystalline cubic Ti-C and hexagonal Ti. The sample Ti-C/Si shows a predominant cubic Ti-C phase (a = 0.4098 lattice parameter with −5.59% relative error). In the case of Ti-C-Al/Si, the lattice parameter was a = 0.41664 nm, with relative error 2.8% for Al phase, and a = 0.5246 nm (−3.5% relative error) for cubic Si. The free surface energy's values are 43.89 mJ/m^2 for the Ti-Ag films and 38.3 mJ/m^2 for the Ti-C film, respectively. The measurements for ternary films showed a hydrophobic character and the free surface energy values were of 13.66 mJ/m^2 for the Ti-C-Ag and 26.14 mJ/m^2 for the Ti-C-Al. The wear rate for Ti-C-Ag was 1.31 × 10^{-7} mm^3/N m (F = 2 N), while in the case of Ti-C-Al coating the wear rate was 4.24 × 10^{-7} mm^3/N m. On the other hand, by increasing the normal load to 3 N, an increase to the wear rate was observed for Ti-C-Ag: 2.58 × 10^{-5} mm^3 compared to 2.33 × 10^{-6} mm^3 for Ti-C-Al coating. TVA technology provides a suitable, inexpensive method of coating, with high productive efficiency, being feasible for further mass production in industrial applications.

Acknowledgments: This work was supported by a grant of Ministry of Research and Innovation, CNDI–UEFISCDI, project 70/2017, PN-III-P4-ID-PCE-2016-0750 within PNCDI III and by a grant of the Romanian National Authority for Scientific Research—ANCS, "Nucleu INFLPR 2018".

Author Contributions: R.V. and A.M. conceived and designed the experiments; V.D. and C.P. performed the experiments; G.P. analyzed the TEM data; P.D. contributed to tribological and wear resistance analysis tools; R.V. wrote the paper.

Conflicts of Interest: The authors declare no conflict of interest.

References

1. Lee, K.; Jeong, Y.-H.; Brantley, W. A.; Choe, H.-C. Surface characteristics of hydroxyapatite films deposited on anodized titanium by an electrochemical method. *Thin Solid Films* **2013**, *546*, 185–188. [CrossRef]
2. Yang, C.; Jiang, B.; Liu, Z.; Feng, L.; Hao, J. Nanocrystalline titanium films deposited via thermal-emission-enhanced magnetron sputtering. *Thin Solid Films* **2015**, *597*, 117–124. [CrossRef]
3. Cordill, M.J.; Taylor, A.A. Thickness effect on the fracture and delamination of titanium films. *Thin Solid Films* **2015**, *589*, 209–214. [CrossRef]
4. Caschera, D.; Federici, F.; Pandolfi, L.; Kaciulis, S.; Sebastiani, M.; Bemporad, E.; Padeletti, G. Effect of composition on mechanical behaviour of diamond-like carbon coatings modified with titanium. *Thin Solid Films* **2011**, *519*, 3061–3067. [CrossRef]
5. Sarkar, J.; McDonald, P.; Gilman, P. Surface characteristics of titanium targets and their relevance to sputtering performance. *Thin Solid Films* **2009**, *517*, 1970–1976. [CrossRef]
6. El-Hossary, F.M.; Negm, N.Z.; Khalil, S.M.; Raaif, M. Surface modification of titanium by radio frequency plasma nitriding. *Thin Solid Films* **2006**, *497*, 196–202. [CrossRef]

7. Zábranský, L.; Buršíková, V.; Daniel, J.; Souček, P.; Vašina, P.; Dugáček, J.; St'ahel, P.; Caha, O.; Buršík, J.; Peřina, V. Comparative analysis of thermal stability of two different nc-TiC/a-C:H coatings. *Surf. Coat. Technol.* **2015**, *267*, 32–39. [CrossRef]
8. Bai, W.Q.; Wang, X.L.; Gu, C.D.; Tu, J.P. Influence of duty cycle on microstructure, tribological and corrosion behaviors of a-C/a-C:Ti multilayer films. *Thin Solid Films* **2015**, *584*, 214–221. [CrossRef]
9. Bai, W.Q.; Li, L.L.; Wang, X.L.; He, F.F.; Liu, D.G.; Jin, G.; Tu, J.P. Effects of Ti content on microstructure, mechanical and tribological properties of Ti-doped amorphous carbon multilayer films. *Surf. Coat. Technol.* **2015**, *266*, 70–78. [CrossRef]
10. Braic, M.; Zoita, N.C.; Danila, M.; Grigorescu, C.E.A.; Logofatu, C. Hetero-epitaxial growth of TiC films on MgO(001) at 100 °C by DC reactive magnetron sputtering. *Thin Solid Films* **2015**, *589*, 590–596. [CrossRef]
11. Li, Q.H.; Savalani, M.M.; Zhang, Q.M.; Huo, L. High temperature wear characteristics of TiC composite coatings formed by laser cladding with CNT additives. *Surf. Coat. Technol.* **2014**, *239*, 206–211. [CrossRef]
12. Kumar, N.; Natarajan, G.; Dumpala, R.; Pandian, R.; Bahuguna, A.; Srivastava, S.K.; Ravindran, T.R.; Rajagopalan, S.; Dash, S.; Tyagi, A.K.; et al. Microstructure and phase composition dependent tribological properties of TiC/a-C nanocomposite thin films. *Surf. Coat. Technol.* **2014**, *258*, 557–565. [CrossRef]
13. Kumar, N.; Natarajan, G.; Kumar, D.D.; Krishna, N.G.; Ravindran, T.R.; Dash, S.; Tyagi, A.K. Wear resistant multiphase compound of Ti(C,O,N)/a-C:H nanocomposite film. *Thin Solid Films* **2015**, *590*, 17–27. [CrossRef]
14. Hossein-Babaei, F.; Rahbarpour, S. Titanium and silver contacts on thermally oxidized titanium chip: Electrical and gas sensing properties. *Solid-State Electron.* **2011**, *56*, 185–190. [CrossRef]
15. Damm, C.; Israel, G. Photoelectric properties and photocatalytic activity of silver-coated titanium dioxides. *Dyes Pigments* **2007**, *75*, 612–618. [CrossRef]
16. Guo, C.; Chen, J.; Zhou, J.; Zhao, J.; Wang, L.; Yu, Y.; Zhou, H. Microstructure and tribological properties of TiAg intermetallic compound coating. *Appl. Surf. Sci.* **2011**, *257*, 10692–10698. [CrossRef]
17. Cao, H.; Liu, X.; Meng, F.; Chu, P.K. Biological actions of silver nanoparticles embedded in titanium controlled by micro-galvanic effects. *Biomaterials* **2011**, *32*, 693–705. [CrossRef] [PubMed]
18. Song, D.-H.; Uhm, S.-H.; Lee, S.-B.; Han, J.-G.; Kim, K.-N. Antimicrobial silver-containing titanium oxide nanocomposite coatings by a reactive magnetron sputtering. *Thin Solid Films* **2011**, *519*, 7079–7085. [CrossRef]
19. Wang, Z.; Cai, X.; Chen, Q.; Chu, P. K. Effects of Ti transition layer on stability of silver/titanium dioxide multilayered structure. *Thin Solid Films* **2007**, *515*, 3146–3150. [CrossRef]
20. Kerti, I. Production of TiC reinforced-aluminum composites with the addition of elemental carbon. *Mater. Lett.* **2005**, *59*, 3795–3800. [CrossRef]
21. Song, M.S.; Huang, B.; Zhang, M.X.; Li, J.G. Study of formation behavior of TiC ceramic obtained by self-propagating high-temperature synthesis from Al–Ti–C elemental powders. *Int. J. Refract. Met. Hard Mater.* **2009**, *27*, 584–589. [CrossRef]
22. Xiao, G.; Fan, Q.; Gu, M.; Jin, Z. Microstructural evolution during the combustion synthesis of TiC–Al cermet with larger metallic particles. *Mater. Sci. Eng. A* **2006**, *425*, 318–325. [CrossRef]
23. Song, M.S.; Zhang, M.X.; Zhang, S.G.; Huang, B.; Li, J.G. In situ fabrication of TiC particulates locally reinforced aluminium matrix composites by self-propagating reaction during casting. *Mater. Sci. Eng. A* **2008**, *473*, 166–171. [CrossRef]
24. Lauridsen, J.; Eklund, P.; Jensen, J.; Hultman, L. Effects of A-elements (A = Si, Ge or Sn) on the structure and electrical contact properties of Ti–A–C–Ag nanocomposites. *Solid Films* **2012**, *520*, 5128–5136. [CrossRef]
25. Sarius, N.G.; Lauridsen, J.; Lewin, E.; Lu, J.; Högberg, H.; Öberg, A.; Ljungcrantz, H.; Leisner, P.; Eklund, P.; Hultman, L. Ni and Ti diffusion barrier layers between Ti–Si–C and Ti–Si–C–Ag nanocomposite coatings and Cu-based substrates. *Surf. Coat. Technol.* **2012**, *206*, 2558–2565. [CrossRef]
26. Almeida Alves, C.F.; Oliveira, F.; Carvalho, I.; Piedade, A.P.; Carvalho, S. Influence of albumin on the tribological behavior of Ag–Ti (C, N) thin films for orthopedic implants. *Mater. Sci. Eng. C* **2014**, *34*, 22–28. [CrossRef] [PubMed]
27. Musa, G.; Ehrich, H.; Mausbach, M. Studies on thermionic cathode anodic vacuum arcs. *J. Vac. Sci. Technol. A* **1994**, *12*, 2887–2895. [CrossRef]
28. Vladoiu, R.; Mandes, A.; Dinca-Balan, V.; Prodan, G.; Kudrna, P.; Tichy, M. Magnesium plasma diagnostics by heated probe and characterization of the Mg thin films deposited by thermionic vacuum arc technology. *Plasma Sources Sci. Technol.* **2015**, *24*, 035008. [CrossRef]

29. Mandes, A.; Vladoiu, R.; Dinca, V.; Prodan, G. Binary C-Ag Plasma breakdown and structural characterization of the deposited thin films by thermionic vacuum arc (TVA) method. *IEEE Trans. Plasma Sci.* **2014**, *42*, 2806–2807. [CrossRef]
30. Ciupina, V.; Morjan, I.; Vladoiu, R.; Nicolescu, V. Application of carbon-tungsten, carbon-beryllium and carbon-aluminium nanostructures in divertors coatings from fusion reactor. *J. Optoelectron. Adv. Mater.* **2013**, *15*, 1450–1456.
31. Ciupina, V.; Vladoiu, R.; Popov, P.; Dinca, V.; Contulov, M.; Mandes, A.; Lungu, C.P. Characterization of nanostructured TiC thin films synthesized by TVA (Thermionic Vacuum Arc) method. *J. Mater. Sci. Eng. A* **2012**, *2*, 16–21.
32. Vladoiu, R.; Ciupina, V.; Mandes, A.; Dinca, V.; Prodan, M.; Musa, G. Growth and characteristics of tantalum oxide thin films deposited using Thermionic Vacuum Arc (TVA) technology. *J. Appl. Phys.* **2010**, *108*, 093301. [CrossRef]
33. Vladoiu, R.; Mandes, A.; Dinca, V.; Contulov, M.; Ciupina, V.; Lungu, C.P.; Musa, G. *Industrial Plasma Technology: Applications from Environmental to Energy Technologies*; Wiley-VCH: Weinheim, Germany, 2010; pp. 357–365.
34. Worner, H.W. The structure of the titanium-silver alloys in the range 0–30 at % silver. *J. Inst. Met.* **1953**, *82*, 222–226.
35. Van Thyne, R.J.; Kessler, H.D.; Rostoker, W. Observations on the Ti Ag. *J. Met.* **1953**, *197*, 670–671.
36. Wyckoff, R.W.G. WWW-MINCRYST, SILVER-4219. *Cryst. Struct.* **1963**, *1*, 7–10.
37. Wyckoff, R.W.G. WWW-MINCRYST, TITANIUM-4770. *Cryst. Struct.* **1963**, *1*, 9–11.
38. Christensen, A.N. The Temperature Factor Parameters of Some Transition Metal Carbides and Nitrides by Single Crystal X-ray and Neutron Diffraction. *Acta Chem. Scand. A* **1978**, *32*, 89–90. [CrossRef]
39. Patterson, A.L. The Scherrer formula for X-ray particle size determination. *Phys. Rev.* **1939**, *56*, 978. [CrossRef]
40. Langford, J.I. The accuracy of cell dimensions determined by Cohen's method of least squares and the systematic indexing of powder data. *J. Appl. Cryst.* **1973**, *6*, 190–196. [CrossRef]
41. Nelson, J.B.; Riley, D.P. An experimental investigation of extrapolation methods in the derivation of accurate unit-cell dimensions of crystals. *Proc. Phys. Soc.* **1945**, *57*, 160–176. [CrossRef]
42. Braun, J.; Ellner, M.; Predel, B. ZurStruktur der Hochtemperaturphase $Ti_{1-x}AI_{1+x}$. *J. Alloys Compd.* **1994**, *203*, 189–193. [CrossRef]
43. Wyckoff, R.W.G. WWW-MINCRYST, TITANIUM-4771. *Cryst. Struct.* **1963**, *1*, 9–11.
44. Wyckoff, R.W.G. WWW-MINCRYST, ALUMINIUM-136. *Cryst. Struct.* **1963**, *1*, 7–10.